# Microstripline-Slotline Transition Analysis Using the Spectral Domain Technique

Yahia M. M. Antar, *Senior Member, IEEE,* Arun K. Bhattcharyya, *Senior Member, IEEE,* and Apisak Ittipiboon, *Member, IEEE*

***Abstract*—A spectral domain analysis of microstripline-slotline transition is presented. The equivalent circuit of the transition is obtained. Elements of the equivalent circuit are determined from the residue theorem. The reflection loss of the transition is determined using the present theory and is found to agree with the experimental data.**

## I. Introduction

MICROSTRIPLINE-slotline transitions have a number of useful applications in microwave devices such as microwave pulse inverters, hybrids, etc. [1]. Using a microstrip-slot transition, one can transfer r.f. power from a microstripline to a slotline and this provides an additional degree of freedom to the microwave integrated circuit designer. Investigations of microstriplines and slotlines are reported in the open literature [1]—[5]. Approximate analysis of microstrip-slot transition including experimental results are also published [6], [7]. The analysis presented in [6] is limited since it only is valid for orthogonal transitions. No general theory which includes the effects of various parameters such as slotline orientation, slotline width, microstripline width, substrate thickness etc. is available.

In this paper, a spectral domain analysis [8] of a microstrip-slot junction is carried out. In this analysis, we consider that the two transmission lines are oriented at an arbitrary angle (Fig. 1). It is found that by adjusting this angle, it is possible to design a perfect transition (with minimum reflection loss) between the two transmission lines. The four-port equivalent circuit of the transition is developed. Elements in the equivalent circuit are obtained employing the residue theorem. For low frequencies and for the special case of orthogonal transition, the equivalent circuit agrees with that reported in [6] primarily due to the fact that the analysis in [6] is based on the quasi-static approximation. For high frequency and for any other angle, the results differ considerably and the present analysis provides more accurate results. The theory is applied to a case for which experimental data is available. The agreement between the present theory and the experiment is good. Variations of the circuit elements values with various parameters are shown.

Manuscript received May 30, 1991; revised October 22, 1991.

Y. M. M. Antar is with the Electrical and Computer Engineering Department, Royal Military College of Canada, Kingston, ON K7K 5L0, Canada.

A. K. Bhattcharyya was with the Electrical Engineering Department, University of Saskatchewan, Saskatoon, SK, Canada. He is presently with the Space and Communications Group, Hughes Aircraft Company, Los Angeles, CA.

A. Ittipiboon is with the Communications Research Centre, Department of Communications, Ottawa, ON, K2H 8S2 Canada.

IEEE Log Number 9105700.

## II. Formulation

In this section, the equivalent circuit for a microstripline-slotline transition will be obtained. The slotline is assumed to be inclined at an angle $90° + \theta_s$ with the microstripline (Fig. 1).

In order to simplify the analysis we assume that the microstripline and the slotline are of infinite extent in both directions. In such a situation, the transverse electric field component on the slot opening will take the following form (a time dependence of exp ($j\omega t$) is assumed):

$$E_{sy'} = E_s \exp(-j\beta_s x'), \qquad x' > 0 \tag{1a}$$

$$= E_s \exp(j\beta_s x'), \qquad x' \leq 0 \tag{1b}$$

where $\beta_s$ is the propagation constant of the slotline. Let the electric and magnetic field vectors of the microstripline before and after the slot junction be

$$\vec{E}^- = V_m \{\exp(-j\beta_m x) + \Gamma \exp(j\beta_m x)\} \vec{e}(y, z) \tag{2a}$$

$$\vec{H}^- = V_m Y_m \{\exp(-j\beta_m x) + \Gamma \exp(j\beta_m x)\} \vec{h}(y, z) \tag{2b}$$

$$\vec{E}^+ = V_m T \exp(-j\beta_m x) \vec{e}(y, z) \tag{3a}$$

$$\vec{H}^+ = V_m T Y_m \exp(-j\beta_m x) \vec{h}(y, z). \tag{3b}$$

In the above equations, $\vec{E}^-$, $\vec{H}^-$ represent EM fields in the region $x < x_1$ and $\vec{E}^+$, $\vec{H}^+$ represent the fields in $x > x_2$ region. The source is located at $x = -\infty$. $V_m$ is the amplitude of the incident voltage and $\Gamma$ is the reflection coefficient caused by the slotline discontinuity. $Y_m$ and $\beta_m$ are the characteristic admittance and the propagation constant respectively, of the microstripline, $\vec{e}(y, z)$ and $\vec{h}(y, z)$ are the normalized modal vectors of the microstrip transmission line. The normalization condition is

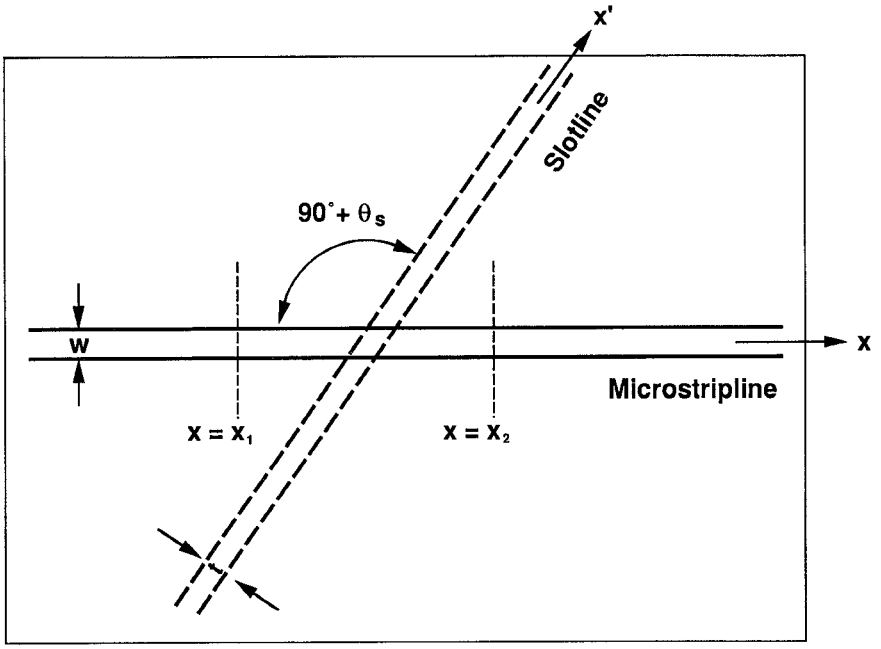


Fig 1. Geometry of the transition.

given by

$$\int_{-\infty}^{\infty}\int \vec{e}(y, z) \times \vec{h}(y, z) \cdot \hat{x}\, dy\, dz = 1 \tag{4}$$

Expressions for $\vec{e}$ and $\vec{h}$ are derived in Appendix I, using the integral transformation technique.

The unknown reflection coefficient $\Gamma$, and the transmission coefficient $T$, in (2) and (3) are obtained using reciprocity [9]. To that end, consider an auxiliary source located at $x = -\infty$, for which the fields are

$$\vec{E}_a = \exp(-j\beta_m x)\, \vec{e}(y, z) \tag{5a}$$

$$\vec{H}_a = Y_m \exp(-j\beta_m x)\, \vec{h}(y, z) \tag{5b}$$

Invoking the reciprocity theorem

$$\oint_s \vec{E}_a \times \vec{H} \cdot \vec{ds} = \oint_s \vec{E} \times \vec{H}_a \cdot \vec{ds},$$

with $\vec{E}$, $\vec{H}$ as the fields of the microstripline given in (2) and (3) and $s$ as the closed surface formed by the planes $x = x_1$, $x = x_2$, $z = 0$ and $z = \infty$, one obtains

$$2\Gamma \int_0^{\infty}\int_{-\infty}^{\infty} \vec{e}(y, z) \times \vec{h}(y, z)\, dy\, dz = -\frac{1}{V_m}\int\int_{\text{slot}} \vec{E}_s \times \vec{h} \exp(-j\beta_m x) \cdot \hat{z}\, ds \tag{6}$$

Using the normalization condition in (4), $\Gamma$ is obtained as

$$\Gamma = -\frac{1}{2V_m}\int\int_{\text{slot}} \vec{E}_s \times \vec{h} \cdot \hat{z} \exp(-j\beta_m x)\, ds, \tag{7}$$

where the integration is taken over the slotline opening. In a similar way, the transmission coefficient $T$ can be determined. The auxiliary source, in that case, should be placed at $x = \infty$, so that the guided fields are

$$\vec{E}_a = \exp(j\beta_m x)\, \vec{e}(y, z)$$

$$\vec{H}_a = Y_m \exp(j\beta_m x)\, \vec{h}(y, z).$$

Using reciprocity once again, the expression for $T$ is obtained as

$$T = 1 + \frac{1}{2V_m}\int\int_{\text{slot}} \vec{E}_s \times \vec{h} \cdot \hat{z} \exp(j\beta_m x)\, ds. \tag{8}$$

After some algebraic manipulations, $\Gamma$ and $T$ can be expressed as

$$\Gamma = -\frac{V_s}{2V_m}[T_1 \cos\theta_s + T_2 \sin\theta_s] \tag{9}$$

$$T = 1 + \frac{V_s}{2V_m}[T_1 \cos\theta_s - T_2 \sin\theta_s] \tag{10}$$

In the above equations, $V_s$ represents the voltage induced on the slotline at $x' = 0$ location which is equal to $V_s = -E_s t$, $t$ being the width of the slot line. $T_1$ and $T_2$ are two infinite integrals given by

$$T_1 = \int_{-\infty}^{\infty} h_y(y, 0) \exp(-j\beta_m \sin\theta_s x' - j\beta_s|x'|)\, dx' \tag{11}$$

$$T_2 = \int_{-\infty}^{\infty} h_x(y, 0) \exp(-j\beta_m \sin\theta x' - j\beta_s|x'|)\, dx' \tag{12}$$

where $h_x$ and $h_y$ are the $x$ and $y$ components of the modal vector $\vec{h}(y, z)$. Expressing $h_y$ in terms of its Fourier transform

$$h_y = \int_{-\infty}^{\infty} \tilde{h}_y(k_y, z) \exp(-jk_y z)\, dk_y$$

and substituting in (11) one obtains the expression for $T_1$ as

$$T_1 = 2j\beta_s \int_{-\infty}^{\infty} \frac{\tilde{h}_y(k_y, 0)}{\{(k_y \cos\theta_s + \beta_m \sin\theta_s)^2 - \beta_s^2\}}\, dk_y. \tag{13}$$

In order to obtain the above expression for $T_1$, it was assumed that the imaginary part of $\beta_s$ is less than zero. Similarly, $T_2$ can be expressed as

$$T_2 = 2j\beta_s \int_{-\infty}^{\infty} \frac{\tilde{h}_x(k_y, 0)}{\{(k_y \cos\theta_s + \beta_m \sin\theta_s)^2 - \beta_s^2\}}\, dk_y \tag{14}$$

Expressions for $\tilde{h}_x$ and $\tilde{h}_y$ are derived in Appendix I.

### A. Equivalent Circuit

It can be noted from (9) and (10) that when $\theta_s = 0$, i.e., the slotline and the microstripline are mutually perpendicular to each other, $T = 1 - \Gamma$. This implies that the line currents on the microstripline before and after the slot discontinuity are equal. In such a case, the equivalent circuit consists of a series impedance only. In other cases, ($\theta_s \neq 0$) the above condition does not hold, so that the equivalent circuit is a general $\pi$-network as shown in Fig. 2. The above equivalent circuit is a consequence of a mathematical derivation, which is outlined in this section.

In order to obtain the equivalent circuit representation of the junction, we first determine the discontinuity of the line voltage caused by the slotline. The discontinuity $\Delta V$ is given by

$$\Delta V = (1 + \Gamma) V_m - T V_m. \tag{15}$$

Substituting (9) and (10) in (15), one obtains

$$\frac{\Delta V}{V_s} = -T_1 \cos\theta_s. \tag{16}$$

Since $T_1$ is complex in general, there exists a phase difference between the slot voltage $V_s$ and the line voltage $\Delta V$. This indicates that the series elements in the equivalent $\pi$-network must contain a reactive load, $jX_s$, in series with an ideal transformer (cf., Fig. 2). The voltage drop across the transformer is responsible for the voltage induced on the slot line. The expressions for the turns ratio $n$, of the transformer and $X_s$ can be determined from the following relation:

$$\frac{n^2 Z_{\text{slot}} + jX_s}{nZ_{\text{slot}}} = -T_1 \cos\theta_s = \gamma + j\delta, \tag{17}$$

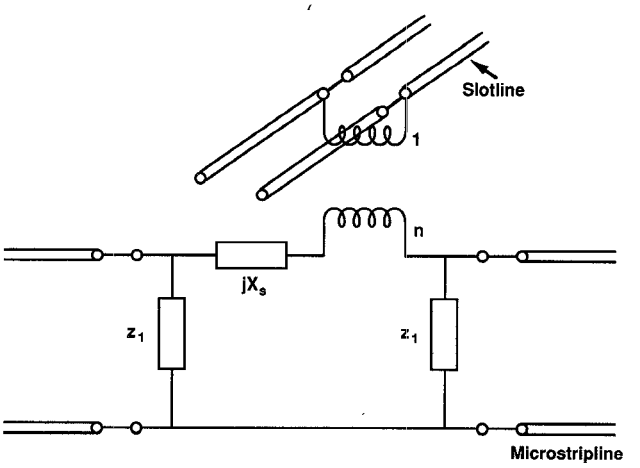


Fig. 2. Equivalent circuit for the transition.

where $Z_{\text{slot}}$ is the equivalent impedance at the microstrip junction offered by the slotline, which is equal to $Z_{os}/2$, where $Z_{os}$ is the characteristic impedance of the slotline. Assuming $Z_{os}$ real, we obtain

$$n = \gamma = \text{Real}(-T_1 \cos\theta_s) \tag{18}$$

$$X_s = \tfrac{1}{2} n\delta Z_{os} = \tfrac{1}{2}\gamma\delta Z_{os}. \tag{19}$$

The shunt impedance $Z_1$ is determined from the discontinuity of the line current. The expression for $Z_1$ is obtained from the relation

$$\bar{Z}_1 = \frac{Z_1}{Z_{om}} = \frac{1 + \Gamma + T}{1 - \Gamma - T},$$

which after substituting the expressions for $\Gamma$ and $T$ becomes

$$\bar{Z}_1 = \frac{2 - RT_2 \sin\theta_s}{RT_2 \cos\theta_s} \tag{20}$$

where $R = V_s/V_m$ and $Z_{om}$ is the characteristic impedance of the microstripline ($Z_{om} = 1/Y_m$). The unknown factor $R$ is a solution of the following equation:

$$\bar{y}_{12} = \frac{-2T}{(1 + \Gamma)^2 - T^2} = \frac{Z_{om}}{jX_s + \gamma^2 \dfrac{Z_{os}}{2}}. \tag{21}$$

The exact expression for $R$ is found to be lengthy. However, with a reasonable assumption, $T_2 \ll T_1$, which is found numerically, and combining (21), (9), and (10), a simplified expression for $R$ is obtained.

$$R = \frac{1}{(\bar{y}_{12} - \frac{1}{2}) T_1 \cos\theta_s}$$

substituting $R$ in (20) we obtain $\bar{Z}_1$.

It is to be noted that in order to determine the numerical values of the components, the infinite integrals in (13) and (14) are to be evaluated. These integrals have a number of singularities arising from the poles of the functions $\tilde{h}_x$, $\tilde{h}_y$ and the zeros of the factor in the denominator (cf., (13) and (14)). In addition, there are branch points at $k_y =$

$\pm j\sqrt{\beta_m^2 - k_o^2}$ for both the integrals. For small dielectric thickness, the contribution around the branch cut (c.f. Fig. 9) is negligible as compared to that contributed by the poles. The closed form expression for $T_1$ and $T_2$ are determined in Appendix II.

## III. Results and Discussion

In order to validate the present formulation, we computed the turns ratio $n$ using (18). To compute the values for $T_1$, (A18), (A19) and (A20) in Appendix II were used. The parameters considered were $\epsilon_r = 10$, $W = 0.3$ cm, $f = 5$ GHz, $t = 0.15$ cm and $\theta_s = 0$. The turns ratio was also computed from formula available in the literature [6, eqn. 3]. The same set of parameters were taken. Fig. 3 shows the variations of $n$ with the substrate thickness $h$. The agreement between the present formulation and that available in the literature is good. The present formulation is expected to be more accurate since the effects of all parameters are taken into consideration. The formula in [6] however does not include any effect of the microstripline width, $W$.

Fig. 4 shows the variations of the turns ratio $n$ with the angle of inclination of the slotline. When the two lines are perpendicular to each other ($\theta_s = 0$), the value of $n$ is maximum. It decreases monotonically with $\theta_s$. The value of $n$ also increases when $h$, the substrate thickness, decreases, which is expected. The value of $n$ does not change appreciably when $\epsilon_r$ varies from 10 to 15. This plot is important for designing slotline-microstripline transitions, since the turns ratio $n$ decides the reflected load seen by the microstripline for a given slotline dimensions. The angle $\theta_s$ can be adjusted to have the maximum coupling over a frequency band.

The normalized series reactance $X_s$ versus $\theta_s$ is plotted in Fig. 5. The substrate thickness was taken as a parameter. The absolute value of $X_s$ decreases with $\theta_s$. The more the substrate thickness, the more is the magnitude of $X_s$. Near $\theta_s = 0$, the value of $X_s$ is substantial. This plot will be useful to decide the extra length of the open circuit matching stub at a given frequency.

Fig. 6 shows the variations of $n$ and normalized $X_s$ for a microstripline-slot line transition on alumina ($\epsilon_r = 9.7$) substrate. The substrate thickness was 0.5 mm and the width of the microstripline was taken as 0.5 mm in order to have a characteristic impedance of approximately 50 Ω. It is found that the value of $n$ varies slightly over the 1 to 10 GHz frequency range. The magnitude of $X_s$ increases (in the negative direction) initially and then becomes almost flat. This plot would be useful to estimate the length of the stub to be used to have a perfect matched transition. Furthermore, since $X_s$ and $n$ do not change appreciably with frequency (especially in the high frequency region) a wide band transition is possible to achieve.

The variations of the normalized shunt susceptance, $y_1$ against $\theta_s$ is plotted in Fig. 7. The magnitude of $y_1$ starts at zero, reaches a maximum and then decreases. When $\theta_s = 0$, $y_1 = 0$ indicating that for two orthogonal lines, the shunt element is absent. However, when $\theta_s \neq 0$, the magnitude of $y_1$ is comparable to $Y_{om}$, the characteristic admittance of the microstripline. Therefore, in order to ob-

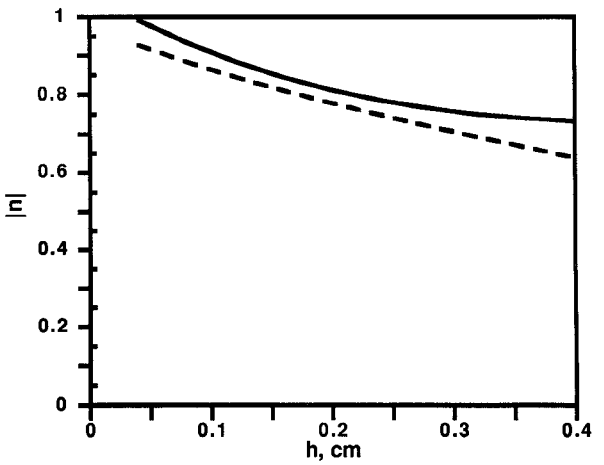


Fig. 3. Turns ratio $n$ versus the substrate thickness. (—— Knorr [6], ——— present theory), ($\epsilon_r = 10$, $w = 0.3$ cm, $f = 5$ GHz, $t = 0.159$ cm, $\theta_s = 0°$).

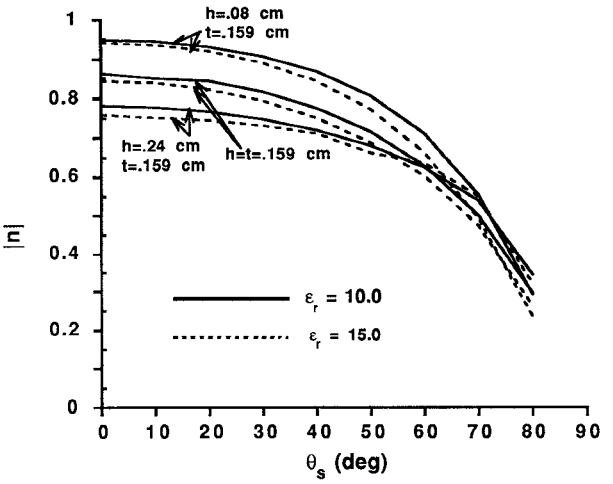


Fig. 4. Variation of the turns ratio $n$ with the angle of inclination $\theta$, ($f = 5$ GHz, $W = 0.2$ cm, $t = 0.159$ cm).

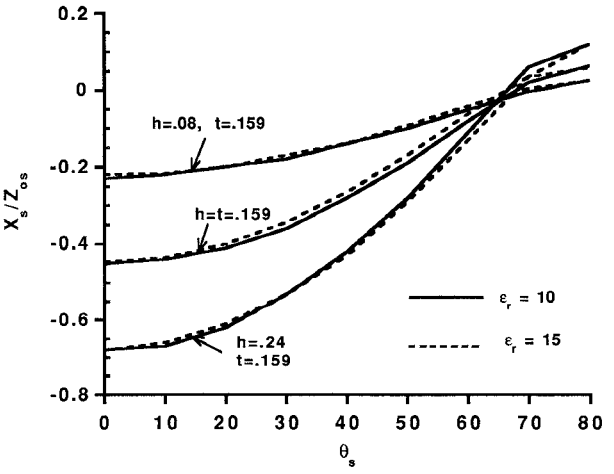


Fig. 5. Series reactance versus $\theta_s$ ($W = 0.2$ cm, $t = 0.159$ cm, $f = 5$ GHz).

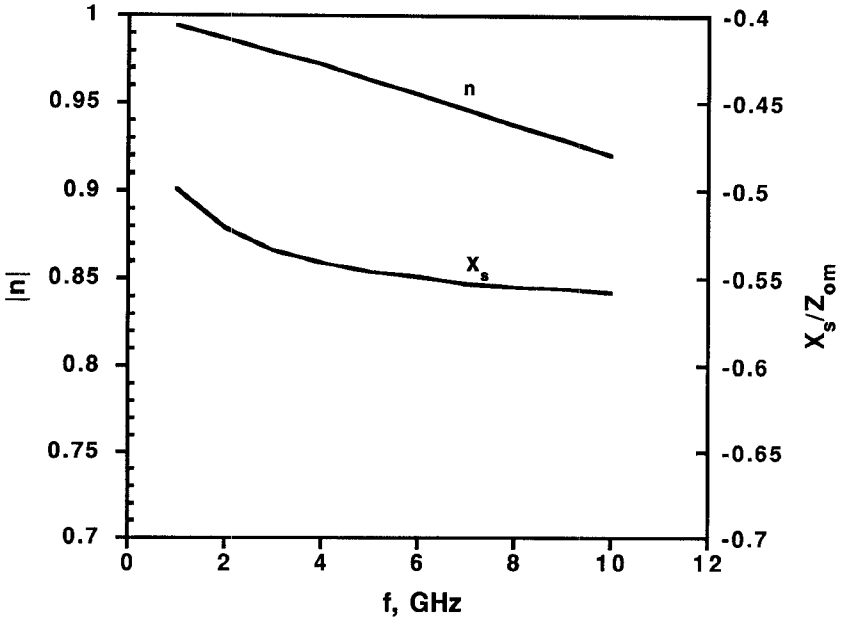


Fig. 6. Variations of $n$ and $X_s$ with frequency for a microstripline-slotline transition on alumina substrate. ($h = W = 0.05$ cm, $\epsilon_r = 9.7$, $t = 0.05$ cm, $\theta_s = 0$).

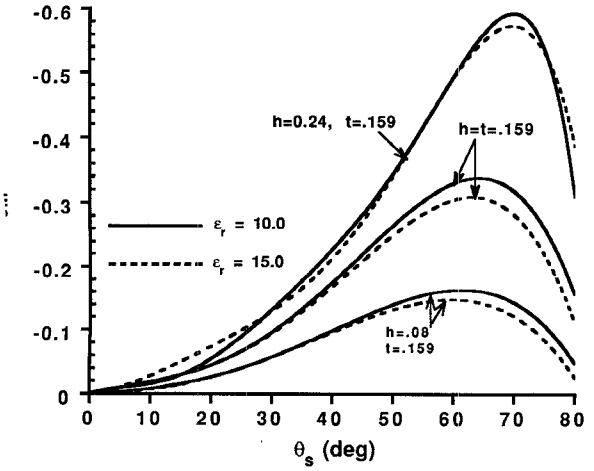


Fig. 7. Normalized shunt susceptance versus $\theta_s$ ($W = 0.2$ cm, $t = 0.159$ cm, $f = 5$ GHz).

tain accurate results, the effect of $y_1$ must be considered. As for the other parameters, here also, the values of $y_1$ does not change much when $\epsilon_r$ changes from 10 to 15, however it increases with an increase in the substrate thickness.

In order to further examine the accuracy of the present model, the input VSWR of a microstripline-slotline transition was computed. The structure under consideration is shown in Fig. 8(a). The physical dimensions of the microstripline and slotline were taken to be the same as in [6]. The stub lengths for the slotline and microstripline were 0.6883 cm each. The end effect of the open ended microstrip was incorporated via an extra length of 0.2h added to the microstripline [1]. For the slotline, the end effect was estimated using Fig. 5.14 of [1]. It is found that this effect can also be incorporated by adding an extra length of 0.134 cm to the slotline near 3 GHz frequency range.

The turns ratio $n$ in the equivalent circuit of the transition was computed as $n = 0.79$ near 3 GHz frequency. The normalized value of $X_s$ was obtained as $1.05\ Z_{os}$. However, in the present case, the slotline being not extended in both directions, therefore the value of $X_s$ should be approximately equal to 50% of the value that is obtained from (19). With these values of $n$ and $X_s$, we determined the input VSWR seen by the microstripline when the slotline is match-terminated at one end. It was noted that when the effect of $X_s$ was ignored, the resonant frequency (frequency for minimum VSWR) was obtained near 2.5 GHz. Inclusion of $X_s$ into consideration moves the resonant frequency to 3.5 GHz (Fig. 8(b)), which agrees with the experimental data [6]. This result indicates the validity and the accuracy of the model presented here.

## IV. Conclusion

A spectral domain analysis of a microstripline-slotline transition is presented. The equivalent circuit, which is a consequence of mathematical results is obtained. The equivalent circuit is used to compute the VSWR of a microstrip-slot transition and the results are found to agree with the experimental data reported [6].

The formulation presented here is rigorous and it incorporates the effects of various parameters such as the dielectric constant of the substrate, microstrip and slotline widths, angle between microstripline and slotline, substrate thickness and frequency. It is found that each of the above parameters has substantial effects on the values of $n$ and $X_s$. The values of $n$ and $X_s$ are very important to design a perfect transition at a given frequency. The value

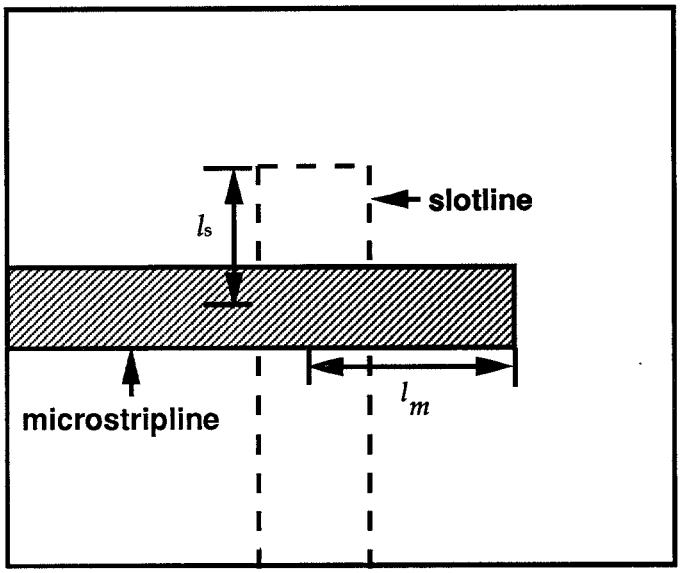


(a)

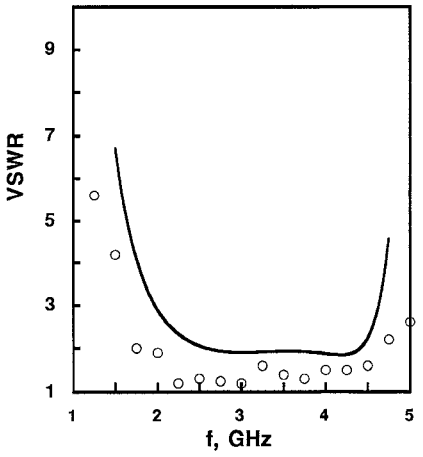


(b)

Fig. 8. (a) Microstripline-slotline transition. (b) Theoretical and experimental VSWR of a microstripline-slotline transition ($l_m = l_s = 0.6883$ cm, $h = 0.318$ cm, $t = 0.207$ cm, $\epsilon_r = 20$). (——— theory, ○ ○, measurements [6]).

of $n$ changes substantially with the angle $\theta_s$, therefore, by adjusting the angle, one can achieve a perfect match between a microstripline and a slotline. Since the theory is based on a dynamic analysis, the results will be useful for high frequency applications, especially at the millimeter wave frequency range.

## Appendix I
## Derivation of the Modal Vectors $\vec{e}(y, z)$ and $\vec{h}(y, z)$ in (4)

Consider a microstripline of width $W$, carrying a current $I_0$. The substrate thickness is $h$ and $\epsilon_f$ is its relative dielectric constant.

In order to derive the expressions for the modal vectors of the above mentioned transmission line, the spectral domain analysis is invoked. The surface current density on the strip can be represented as (for a small width)

$$I_x = \frac{I_0}{W} e^{-j\beta x}, \quad -W/2 < y < W/2, \tag{A1}$$

where $\beta$ is the propagation constant of the microstripline which can be obtained from the following equations [1]:

$$\beta = \frac{2\pi\sqrt{\epsilon_e}}{\lambda_0} \tag{A2}$$

$$\epsilon_e = \frac{\epsilon_f + 1}{2} + \left(\frac{\epsilon_f - 1}{2}\right)\left(1 + \frac{10h}{W}\right)^{-(1/2)} \tag{A3}$$

The surface current $I_x$ will produce the TM and TE fields. The TM field components can be generated from the longitudinal component of the displacement vector $D_z$ which satisfies the following differential equation:

$$\nabla^2 D_z + k^2 D_z = \frac{\partial \rho_e}{\partial z} - \frac{\partial \epsilon}{\partial z}(\nabla_t \cdot \vec{E}_t) \tag{A4}$$

where $k$ is the wave number inside a dielectric layer and $\vec{E}_t$ is the electric field vector in the $Z$ = constant plane. The differential operation $\nabla_t$ is given by

$$\nabla_t = \hat{x}\frac{\partial}{\partial x} + \hat{y}\frac{\partial}{\partial y}.$$

The electric charge density, $\rho_e$, is obtained from the continuity equation and is given by

$$\rho_e = \frac{I_0 \beta}{\omega W} e^{-j\beta x}\delta(z - h), \tag{A5}$$

$\omega$ being the angular frequency.

In order to obtain the solution for $D_z$, (A4) is expressed in the Fourier domain:

$$\frac{d^2\tilde{D}_z}{dz^2} + k_z^2 \tilde{D}_z = \frac{\partial \tilde{\rho}_e}{\partial z} - \frac{\partial \epsilon}{\partial z}\tilde{I} \tag{A6}$$

where

$$D_z = e^{-j\beta x}\int_{-\infty}^{\infty} \tilde{D}_z(k_y, z)\, e^{-jk_y y}\, dk_y$$

$$\nabla_t \cdot \vec{E}_t = e^{-j\beta x}\int_{-\infty}^{\infty} \tilde{I}(k_y, z)\, e^{jk_y y}\, dk_y$$

$$\rho_e = e^{-j\beta x}\int_{-\infty}^{\infty} \tilde{\rho}_e(k_y, z)\, e^{-jk_y y}\, dk_y$$

$$k_z^2 = k^2 - k_y^2 - \beta^2.$$

The divergence equation in the spectral domain yields

$$\frac{d\tilde{D}_z}{dz} + \epsilon\tilde{I} = \tilde{\rho}_e. \tag{A7}$$

Equations (A6) and (A7) are solved for $\tilde{D}_z$ using the transmission line analogy [8]. The final solution for $\tilde{D}_z$ in the region $0 < z < d$ is obtained as

$$\tilde{D}_z(k_y, z) = -\tilde{D}_z(k_y, 0)\frac{y_{02}}{y_{in}}\frac{\cos(k_{1z}z)}{\cos(k_{1z}h)}$$

where

$$\tilde{D}_z(k_y, 0) = \frac{1}{2\pi}\delta(z - h)\int_{-W/2}^{W/2} \rho_e e^{jk_y y}\, dy$$

$$= \frac{\beta I_0}{2\pi\omega}\frac{\sin(k_y W/2)}{(k_y W/2)} \tag{A8}$$

$y_{02}$ and $y_{in}$ are given by

$$y_{02} = jk_{02}/\epsilon_0,$$

$$y_{in} = y_{02} + jy_{01}\tan(k_{1z}h), \quad y_{01} = jk_{1z}/\epsilon_0\epsilon_f.$$

The TE field components can be determined from the longitudinal component of the magnetic displacement vector, $B_z$. Using a very similar procedure, the expression for $B_z$ in the spectral domain is obtained as

$$\tilde{B}_z(k_y, z) = \frac{\mu v_0' y_{02}' \sin(k_{1z}z)}{k_{1z} y_{in}' \cos(k_{1z}h)} \tag{A9}$$

with

$$v_0' = \frac{1}{2\pi}\int_{-W/2}^{W/2} \hat{z}\cdot(\nabla\times\vec{I})e^{jk_y y}\, dy$$

$$= -\frac{1}{2\pi}\int_{-W/2}^{W/2}\frac{\partial I_x}{\partial y}e^{jk_y y}\, dy = \frac{jk_y I_0}{2\pi}\frac{\sin(k_y W/2)}{(k_y W/2)},$$

$$y_{02}' = -j\mu/k_{0z}, \quad y_{in} = y_{02}' + jy_{01}'\tan(k_{1z}h),$$

$$y_{01}' = -j\mu/k_{1z}.$$

The magnetic field components are obtained from the relation

$$\vec{H} = \nabla\times\vec{A} + \frac{1}{j\omega\mu}(\nabla\times\nabla\times\vec{F}) \tag{A10}$$

where $\vec{A} = \hat{z}A_z$ and $\vec{F} = \hat{z}F_z$ with $\tilde{A}_z = j\omega\tilde{D}_z/(\beta^2 + k_y^2)$ and $\tilde{F}_z = j\omega B_z/(\beta^2 + k_y^2)$.

Using (A10), the expression for $\tilde{H}_x$ and $\tilde{H}_y$ are obtained as

$$\tilde{H}_x = \frac{-\omega k_y}{(k_y^2 + \beta^2)}\tilde{D}_z(k_y, 0)\frac{y_{02}}{y_{in}}\frac{\cos(k_{1z}z)}{\cos(k_{1z}h)}$$

$$- \frac{j\beta}{k_y^2 + \beta^2}v_0'\frac{y_{02}'}{y_{in}'}\frac{\cos(k_{1z}z)}{\cos(k_{1z}h)} \tag{A11}$$

and

$$\tilde{H}_y = \left[\omega\beta\tilde{D}_z(k_y, 0)\frac{y_{02}}{y_{in}} - jk_y v_0'\frac{y_{02}}{y_{in}'}\right]$$

$$\cdot\frac{\cos(k_{1z}z)}{\cos(k_{1z}h)}\cdot\frac{1}{(\beta^2 + k_y^2)}. \tag{A12}$$

The modal current vector $\vec{h}$ is given by $\hat{x}h_x + \hat{y}h_y + \hat{z}h_z$, where $\tilde{h}_x = \tilde{H}_x/I_0$, $\tilde{h}_y = \tilde{H}_y/I_0$ and $\tilde{h}_z = \tilde{B}_z/\mu I_0$. The modal voltage vector $\vec{e}$ can be obtained using the relation

$$\nabla\times\vec{h} = j\omega\epsilon Z_0\vec{e}$$

where $Z_0$ is the characteristic impedance of the transmission line. Note that the factor $Z_0$ is multiplied with $\vec{e}$ to comply with the normalization condition in (4).

## Appendix II
## Evaluations of $T_1$ and $T_2$

The integral for $T_1$ in (13) is given by

$$T_1 = 2j\beta_s\int_{-\infty}^{\infty}\frac{\tilde{h}_y(k_y, 0)}{\{(k_y\cos\theta_s + \beta_m\sin\theta_s)^2 - \beta_s^2\}}\, dky \tag{A13}$$

with

$$\tilde{h}_y(k_y, 0) = \frac{\sin(k_y W/2)}{2\pi(k_y W/2)}\left[\beta_m^2\frac{y_{02}}{y_{in}} + k_y^2\frac{y_{0z}'}{y_{in}'}\right]$$

$$\cdot\frac{1}{\cos(k_{1z}h)(\beta_m^2 + k_y^2)} \tag{A14}$$

$$= \frac{\sin(k_y W/2)}{k_y(\beta_m^2 + k_y^2)}f_y(k_y), \tag{A15}$$

where

$$f_y(k_y) = \frac{1}{\pi W}\left[\beta_m^2\frac{y_{0z}}{y_{in}} + k_y^2\frac{y_{02}'}{y_{in}'}\right]\frac{1}{\cos(k_{1z}h)} \tag{A16}$$

All the terms in the above equations are defined in Appendix I. The term $\tilde{h}_y$ can be expressed in the following exponential form:

$$\tilde{h}_y = \frac{[\exp(jk_y W/2) - \exp(-jk_y W/2)]f_y(k_y)}{2jk_y(\beta_m^2 + k_y^2)} \tag{A17}$$

Substituting (A17) in (A13), one obtains

$$T_1 = 2j\beta_s[T_{1a} - T_{1b}] \tag{A18}$$

with

$$T_{1a} = \frac{1}{2j}\int_{-\infty}^{\infty}\frac{\exp(jk_y W/2)f_y(k_y)}{k_y(\beta_m^2 + k_y^2)(k_y'^2 - \beta_s^2)}\, dk_y \tag{A19}$$

$$T_{2a} = \frac{1}{2j}\int_{-\infty}^{\infty}\frac{\exp(-jk_y W/2)f_y(k_y)}{k_y(\beta_m^2 + k_y^2)(k_y'^2 - \beta_s^2)}\, dk_y \tag{A20}$$

where $k_y' = k\cos\theta_s + \beta_m\sin\theta_s$. The above two integrals have singularities at $k_y = 0$, $\pm j\beta_m$, $\lambda_1$ and $\lambda_2$ where

$$\lambda_1 = (\beta_s - \beta_m\sin\theta_s)/\cos\theta_s$$

$$\lambda_2 = -(\beta_s + \beta_m\sin\theta_s)/\cos\theta_s.$$

Recall that the imaginary part of $\beta_s$ being negative, the poles $\lambda_1$ and $\lambda_2$ are located below and above the real axis, respectively. In addition to those poles, the integrals have two branch points at $k_y = \pm j\sqrt{\beta_m^2 - k_0^2}$. The branch points arise from the multivalued nature of the complex function $f_y(k_y)$.

In order to evaluate $T_{1a}$, we deform the contour as

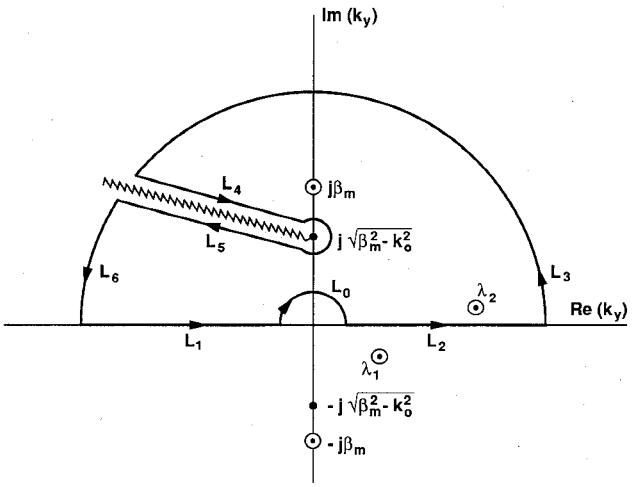


Fig. 9. Contour of integration in the complex $k_y$ plane.

shown in Fig. 9. The integrand in (A19) vanishes on the semicircular segment due to the exponential term. Therefore, from the residue theorem, the integral is obtained as

$$T_{1a} = \frac{1}{2j}\left[\int_{L_0} (I)\, dk_y + 2\pi j\, Res(\lambda_2) + 2\pi j\, Res(j\beta_m) + \int_{L_4+L_5} (I)\, dk_y\right].$$

where $I$ is the integrand. The contributions along the path $L_4 + L_5$ is negligibly small as compared to the rest. Therefore, evaluating the residues, we obtain

$$T_{1a} \simeq \frac{-\pi}{4\beta_s \cos\theta_s}\left[\frac{f_y(0)}{\beta_m^2}\left(\frac{1}{\lambda_1} - \frac{1}{\lambda_2}\right) + \frac{\exp(-\beta_m W/2) f_y(j\beta_m)}{\beta_m^2} \cdot \left\{\frac{1}{(j\beta_m - \lambda_1)} - \frac{1}{(j\beta_m - \lambda_2)}\right\} + \frac{2\exp(j\lambda_2 W/2) f_y(\lambda_2)}{\lambda_2(\beta_m^2 + \lambda_2^2)}\right]. \quad \text{(A21)}$$

Similarly we evalute $T_{1b}$. In that case, the semicircular contour is taken in the lower half of the complex $k_y$-plane. The expression for $T_{1b}$ is obtained as

$$T_{1b} \simeq \frac{\pi}{4\beta_s \cos\theta_s}\left[\frac{f_y(0)}{\beta_m^2}\left(\frac{1}{\lambda_1} - \frac{1}{\lambda_2}\right) - \frac{2\exp(-j\lambda_1 W/2) f_y(\lambda_1)}{\lambda_1(\lambda_1^2 + \beta_m^2)} + \frac{\exp(-\beta_m W/2) f_y(-j\beta_m)}{\beta_m^2} \cdot \left\{\frac{1}{(j\beta_m + \lambda_2)} - \frac{1}{(j\beta_m + \lambda_1)}\right\}\right]. \quad \text{(A22)}$$

Substituting $T_{1a}$ and $T_{1b}$ in (A18) we obtain $T_1$. A similar procedure is used to evaluate $T_2$ and we obtain a very similar expression as in $T_1$, except that $f_y(k_y)$ should be replaced by $f_x(k_y)$ in (A21) and (A22), where

$$f_x(k_y) = -\frac{1}{\pi W} k_y \beta_m \left[\frac{y_{02}}{y_{in}} - \frac{y'_{02}}{y'_{in}}\right] \frac{1}{\cos(k_{1z} h)} \quad \text{(A23)}$$

Substituting $f_x(k_y)$ in all places for $f_y(k_y)$ in (A21) and (A22), we obtain $T_{2a}$ and $T_{2b}$. The integral $T_2$ will be then

$$T_2 = 2j\beta_s (T_{2a} - T_{2b}). \quad \text{(A24)}$$

## Acknowledgment

The authors would like to acknowledge the assistance and encouragement of M. Cuhaci and R. Douville of the Communications Research Centre. The assistance provided by the Department of National Defense (DATES-ARP FUHDI to Y. M. M. Antar) is gratefully acknowledged.

## References

[1] K. C. Gupta, R. Garg, and I. J. Bahl, *Microstrip Lines and Slot Lines*. Norwood, MA: Artech House, 1979.
[2] H. E. Stinehelfer, "An accurate calculation of uniform microstrip transmission line," *IEEE Trans. Microwave Theory Tech.*, vol. MTT-16, pp. 439–444, 1968.
[3] J. B. Knorr and A. Tufekcioglu, "Spectral-domain calculation of microstrip characteristic impedance," *IEEE Trans. Microwave Theory Tech.*, vol. MTT-23, pp. 725–728, 1975.
[4] S. B. Cohn, "Slot line on a dielectric substrate," *IEEE Trans. Microwave Theory Tech.*, vol. MTT-17, pp. 768–778, 1969.
[5] J. B. Knorr and K. D. Kuchler, "Analysis of coupled slots and coplanar strips on dielectric substrates," *IEEE Trans. Microwave Theory Tech.*, vol. MTT-23, pp. 541–548, 1975.
[6] J. B. Knorr, "Slot-line transitions," *IEEE Trans. Microwave Theory Tech.*, vol. MTT-22, pp. 548–554, 1974.
[7] B. Schiek and J. Kohler, "An improved microstrip-to-microstrip transition," *IEEE Trans. Microwave Theory Tech.*, vol. MTT-24, pp. 231–233, 1976.
[8] A. K. Bhattacharyya and R. Garg, "Spectral domain analysis of wall admittances for circular and annular microstrip patches and the effects of surface waves," *IEEE Trans. Microwave Theory Tech.*, vol. AP-33, pp. 1067–1073, 1985.
[9] R. F. Harrington, *Time Harmonic Electromagnetic Fields*. New York: McGraw-Hill, 1961.
[10] R. E. Collin and F. J. Zucker, *Antenna Theory*, pt. I. New York: McGraw-Hill, 1969.

**Yahia M. M. Antar** (S'73–M'76–SM'85) was born on November 18, 1946 in Meit Temmama, Egypt. He received the B.Sc. (Hons.) degree in 1966 from Alexandria University, Egypt, and the M.Sc. and Ph.D. degrees from the University of Manitoba, Winnipeg, Canada, in 1971 and 1975, respectively, all in electrical engineering.

After graduation he joined the Faculty of Engineering at Alexandria, where he was involved in teaching and research. At the University of Manitoba he held a University Fellowship, a National Research Council Postgraduate Scholarship, and later an NRC Postdoctoral Fellowship. In 1976–1977 he was with the Faculty of Engineering at the University of Regina, Canada. In June 1977, he was awarded a Visiting Fellowship from the Government of Canada to work at the Com-

munications Research Centre of the Department of Communications, Shirley's Bay, Ottawa, where he was involved in research and development of satellite technology with the Space Electronics group. In May 1979, he joined the Division of Electrical Engineering, National Research Council of Canada, Ottawa, where he worked on polarization radar applications in remote sensing of precipitation, radio wave propagation, electromagnetic scattering and radar cross section investigations. In November 1987, he joined the staff of the Department of Electrical and Computer Engineering at the Royal Military College of Canada in Kingston, where he is now professor of Electrical Engineering. He has an adjunct appointment at the University of Manitoba and is presently the Chairman of the Canadian CNC, URSI Commission B.

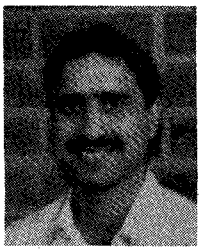

**Arun K. Bhattacharyya** (M'87–SM'91) was born in Painta, Burdwan, India in 1958. He received the B.Eng. (electronics and telecommunication engineering) degree from Bengal Engineering College, University of Calcutta, in 1980, and the M.Tech. and Ph.D. degrees from the Indian Institute of Technology, Kharagpur in 1982 and 1985, respectively. His Ph.D. work was mainly on printed antennas where he developed a technique for analyzing such antennas. He also worked on the spectral domain technique for patch antennas analyses as a part of his Ph.D. research.

From November 1985 to April 1987, he was with the Department of Electrical Engineering, University of Manitoba, as a Postdoctoral Fellow. There he worked on various topics such as microstrip phased array antennas including mutual coupling effects, surface wave coupling between antenna elements, circularly polarized antennas, printed slot arrays, etc. From May 1987 to October 1987 he worked with Til-Tek limited, Kemptville, Canada, as a Senior Antenna Engineer where he designed, fabricated and tested various antennas and arrays. He then joined the University of Saskatchewan, Canada, as an Assistant Professor in the Electrical Engineering Department in November 1987. He was promoted to the Associate Professor rank in 1990. During his stay at the University of Saskatchewan, he worked on finite ground plane effects on the radiation characteristics of patch antennas, spectral domain analysis of multilayered structures, space and surface waves in a layered media, aperture coupled patch antennas, etc. He also taught a number of undergraduate and graduate level courses in the areas of electromagnetics and applied mathematics. Since July 1991, he has been with the Hughes Aircraft Company, Space and Communication group in Los Angeles. His fields of present interest include aperture coupled patch antennas, high frequency characterization of microstriplines and slotlines and their transitions, phased array antennas, etc. He has a number of publications in his research areas.

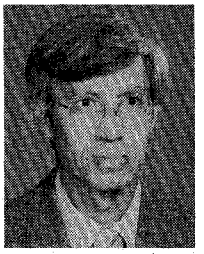

**Apisak Ittipiboon** (M'80) received the B.E.(Hons.) degree from Khonkean University, Thailand, and the M.Sc. and the Ph.D. degrees in electrical engineering from the University of Manitoba, Canada.

In 1985 he joined the Communications Research Centre where he is now a Research Scientist. He has been involved in research and development work on active phased array antennas. His interests include printed circuit antennas, millimeter-wave technology and devices.